Supporting Information

Dielectric morphology engineering: hydrogel electrolyte with balanced local electric field to enhance the migration number of zinc ions

Peng Xie,[#a] Zichen Song, [#a] Zewei Hu,[a] Fuhua Yang,[c] Chao Han,[b] Weijie Li[*a]

a Powder Metallurgy Research Institute, Central South University, Changsha, 410083, China. E-mail: li-306@csu.edu.cn

b School of Materials Sciences and Engineering, Central South University, Changsha, 410083, China

c School of Metallurgy and Environment, Central South University, Changsha, 410083, China

# These authors contributed equally to the article.

1. Experimental Section

1.1 Materials

Zinc trifluoromethanesulfonate ($Zn(CF_3SO_3)_2$) was purchased from Suzhou Duoduo Technology Co., Ltd. Polyvinyl alcohol (PVA) was purchased from Macklin Reagent Co., Ltd. Sodium chloride (NaCl) was purchased from Macklin Reagent Co., Ltd. Vanadium pentoxide (V_2O_5) was purchased from Macklin Reagent Co., Ltd. Titanium dioxide (TiO_2) was purchased from Shanghai Aichun Biotechnology Co., Ltd. Sodium hydroxide (NaOH) was purchased from Aladdin Reagent Co., Ltd. Polyvinylidene fluoride (PVDF) was purchased from Aladdin Reagent Co., Ltd. N-methyl-2-pyrrolidone (NMP) was purchased from Aladdin Reagent Co., Ltd. Acetylene black was purchased from Taiyuan Lizhiyuan Technology Co., Ltd. Hydrochloric acid (HCl) was purchased from Sinopharm Chemical Reagent Co., Ltd. All materials were used without further purification.

1.2 Barium Titanate Nanowires (BTO-NWs)

$BaTiO_3$ nanowires were synthesized via a hydrothermal method. (1) Preparation of $H_2Ti_3O_7$: 0.5 g of TiO_2 was dispersed in 40 mL of NaOH solution (10 mol L^{-1}) and stirred for 1 h. The mixture was transferred into a 100 mL Teflon-lined autoclave and maintained at 210 °C for 24 h. The product was washed with deionized water, then stirred in 0.2 mol L^{-1} dilute HCl for 4 h, and subsequently washed with deionized water and anhydrous ethanol until neutral. The product was collected and vacuum-dried at 60 °C for 12 h to obtain $H_2Ti_3O_7$. (2) Preparation of BTO-NWs: 0.1 g of $H_2Ti_3O_7$ was added to 50 mL of freshly prepared $Ba(OH)_2$ solution (0.05 mol L^{-1}) (atomic ratio Ba:Ti = 2:1). After ultrasonic dispersion for 5 min, the mixture was transferred to a 100 mL autoclave and reacted at 210 °C for 24 h. The product was collected, washed with deionized water and anhydrous ethanol, and completely vacuum-dried at 60 °C to obtain white solid BTO-NWs.

1.3 Barium Titanate Nanoparticles (BTO-NPs)

BTO-NPs were prepared by ball milling treatment. 10 g of commercial $BaTiO_3$ powder was subjected to high-energy ball milling. The ball-to-powder weight ratio was 10:1, and the milling time was 6 h. Barium titanate nanoparticles (BTO-NPs) were thus obtained.

1.4 Barium Titanate Nanosheets (BTO-NTs)

$BaTiO_3$ nanosheets were synthesized via a two-step molten salt method. (1) Precursor preparation: 2 g of BTO-NPs and 3 g of TiO_2 (mass ratio 6:9) were mixed and ball-milled for 12 h. 5 g of NaCl was added to the ball-milled mixture. After thorough grinding, the mixture was calcined at 800 °C for 1 h and then at 1150 °C for 3 h in air to obtain the precursor. (2) The precursor was mixed with BTO-NPs at a mass ratio of 1:1. NaCl with an equal mass to this mixture was added and

mixed uniformly. The mixture was calcined at 800 °C for 1 h, followed by 1170 °C for 5 h, to obtain BTO-NTs.

1.5 Preparation of Hydrogel Electrolytes

PVA-based hydrogel electrolytes (PVA-HE) were prepared using a freeze-thaw cycling method: 1 g of PVA (20 wt% of the deionized water mass) was added to freshly prepared 1 M $Zn(CF_3SO_3)_2$ solution, followed by heating in an oil bath at 90 °C with magnetic stirring for 3 h. Employing an in-situ preparation strategy for the HE, a Zn anode was placed in the cathode shell, and approximately 0.6 mL of the gel was cast. After standing for 24 h, it was frozen at -18 °C for 15 h and then thawed at room temperature for 24 h. Hydrogel electrolytes filled with different fillers were prepared similarly, with 5 wt% (relative to PVA mass) of different types of BTO added, named BTO-NWs-PVA, BTO-NPs-PVA, and BTO-NTs-PVA, respectively.

1.6 Preparation of $NaV_3O_8 \cdot 1.5H_2O$ (NVO)

1 g of V_2O_5 was dispersed in 15 mL of NaCl solution (2 mol L^{-1}) and magnetically stirred at 30 °C for 96 h to obtain a brown-red slurry. The slurry was filtered under vacuum and washed sequentially with deionized water and ethanol. The washed product was collected and vacuum-dried at 80 °C for 12 h to obtain a dark-red powdery solid. The molecular formula of this active material is $NaV_3O_8 \cdot 1.5H_2O$ (NVO).

2. Material Characterization

The morphologies of NVO, BTO-NPs, BTO-NWs, and BTO-NTs were analyzed using scanning electron microscopy (SEM, JEOL JSM-6700). The surface of the Zn anode after electrochemical testing was also analyzed by SEM to investigate the uniformity of Zn deposition/stripping, by-product formation, and dendrite growth after cycling. Phase composition analysis of NVO, BTO-NPs, BTO-NWs, and BTO-NTs was performed using X-ray diffraction (XRD, Bruker D8, Cu Kα radiation). Fourier transform infrared spectroscopy (FTIR, Thermo iN10) was employed to characterize the chemical bond information of different hydrogel electrolytes.

3. Electrochemical Measurements

3.1 Electrochemical Performance Testing

Electrochemical measurements were conducted by assembling CR2032 coin cells, including Zn||Zn symmetric cells, Zn||Cu half-cells, and Zn||NVO full cells, to evaluate electrochemical performance. The zinc foil used had a thickness of 100 μm (151.94 mg). The symmetric cells consisted of two zinc foil electrodes, with the hydrogel serving as both the electrolyte and separator. For performance testing of the pure 1 M $Zn(CF_3SO_3)_2$ aqueous electrolyte, an additional piece of glass fiber paper was used as the separator. For the 20% and 50% depth of discharge (DOD) tests, Zn||Zn cells using the BTO-NPs-PVA hydrogel electrolyte were assembled with a zinc foil thickness of 10 μm (corresponding to 5.9 mA h cm^{-2}). Zn||Cu half-cells, with copper foil as the working electrode and zinc foil as the reference/counter electrode, were assembled to study zinc deposition/stripping behavior. The NVO cathode was prepared by mixing NVO powder, carbon nanotubes (CNTs), and polyvinylidene fluoride (PVDF) in a mass ratio of 7:2:1 using N-methyl-2-pyrrolidone (NMP) as the solvent. The resulting slurry was coated onto a graphite foil current collector (100 μm thickness), and the electrode was dried in a vacuum oven at 90 °C for 12 h. The mass loading of the active material was controlled at ≈1.5 mg cm^{-2}. Pouch cells were assembled using zinc foil as the anode, NVO coated on stainless steel foil as the cathode, and BTO-NPs-PVA as the electrolyte. All assembled cells were allowed to rest for 6 h prior to testing. Electrochemical performance was evaluated using a Neware battery test system (CT-4008Tn-5V10mA-HWX, Shenzhen, China).

3.2 Ionic Conductivity

The ionic conductivity (σ) was calculated from the bulk resistance (R) obtained via electrochemical impedance spectroscopy (EIS) measurements on stainless steel (SS)||hydrogel||SS sandwich-type capacitors. EIS was performed with a perturbation amplitude of 10 mV over a frequency range of 10^{-2} to 10^{6} Hz. The ionic conductivity was calculated using the following formula:

$$\sigma = \frac{L}{RS}$$

σ - Ionic conductivity.

L - Electrolyte thickness.

R - Bulk resistance of the electrolyte.

S - Contact area between the electrolyte and the steel electrode.

3.3 Ion Transference Number

The ion transference number ($t_{(Zn^{2+})}$) was measured using a method combining AC impedance spectroscopy with potentiostatic polarization. The interface impedance and steady-state current of the assembled stainless steel (SS)||hydrogel||SS symmetric cell were measured before and after polarization. The transference number was calculated using the following formula:

$$t_{Zn^{2+}} = \frac{I_s(\Delta V - I_0 R_{el}^0)}{I_0(\Delta V - I_s R_{el}^s)}$$

ΔV - Polarization voltage (10 mV).

I_0 - Initial current before polarization.

I_s - Steady-state current after polarization.

R_0 - Interfacial resistance before polarization.

R_s - Interfacial resistance after polarization.

3.4 Activation Energy

Zn||HE||Zn symmetric cells were assembled. EIS tests were conducted at different temperatures (30, 40, 50, and 60 °C). The activation energy (E_a) was calculated from the slope of the plot of logarithmic conductivity versus reciprocal temperature, based on the Arrhenius formula:

$$\sigma = Ae^{\frac{-E_a}{RT}}$$

σ - Ionic conductivity.

E_a - Activation energy.

A - Pre-exponential factor.

R - Gas constant (8.314 J mol^{-1} K^{-1}).

T - Absolute temperature (K).

4 Simulated calculations

Finite element analysis simulations were conducted using COMSOL Multiphysics software. A potential of 0 V was applied to all anode surfaces, and an average current density of 25 mA cm^{-2} was applied to the cathode surface. The bulk electrolyte conductivity was set to 10^{-3} S/cm. The initial Zn^{2+} ion concentration in the electrolyte was set to 500 mol m^{-3}. To reflect the influence of initial perturbations for the initial electric field distribution calculation, five micro-protrusions were set on the material surface to characterize the effect of initial dendrite nucleation sites.

The finite element model was established based on the law of mass conservation and the assumption of electroneutrality of relevant ions (possible side reactions were not considered). The simulation considered the influence of two different factors on ion concentration: concentration diffusion and electric field migration. A simulation model was established for a local region of 80 × 60 μm, with an initial layer thickness of 5 μm. The study involved three types of models: the first type for the BTO-NWs electrolyte, the second for the BTO-NPs electrolyte, and the third for the BTO-NTs electrolyte. Arrays of squares, circles, and bars were set within the electrolytes to simulate the rectification effect of BTO fillers with different morphologies on ion and electron flows.

Current and concentration distributions were tracked through the current distribution and concentration diffusion equations. The flux of each ion in the electrolyte can be calculated by the Nernst-Planck equation:

$$N_i = -D_i\left(\nabla c_i + \frac{F}{RT} z_i c_i \nabla \emptyset_l\right), i = 1,2,3,\cdots,n$$

where D_i, N_i, c_i, z_i, F, T, R and Φ_l represent the diffusion coefficient, flux, concentration, charge number, Faraday constant, temperature, gas constant, and electrolyte potential, respectively. l denotes the position along the diffusion region of thickness d ($0 < l < d$). Based on the steady-state continuity equation

$$\frac{\partial_{c_i}}{\partial_t} + \nabla * N_i = 0$$

and the electroneutrality assumption

$$F\sum_{i=1}^{n} z_i c_i = 0$$

the boundary condition was set as:

$$\vec{n} \cdot J = 0$$

The simulation steps included two parts: current distribution initialization and steady-state calculation. During the deposition process, ions diffusing to the surface of the deposition layer continuously gain electrons and are reduced to atoms, leading to continuous thickening and protrusion of the deposition layer while simultaneously consuming ions in the electrolyte. Consequently, the ion concentration at the deposition layer surface tends towards zero, while the ion flux and electron density at the dendrite surface reach their maximum values.

5 Supplementary Figures

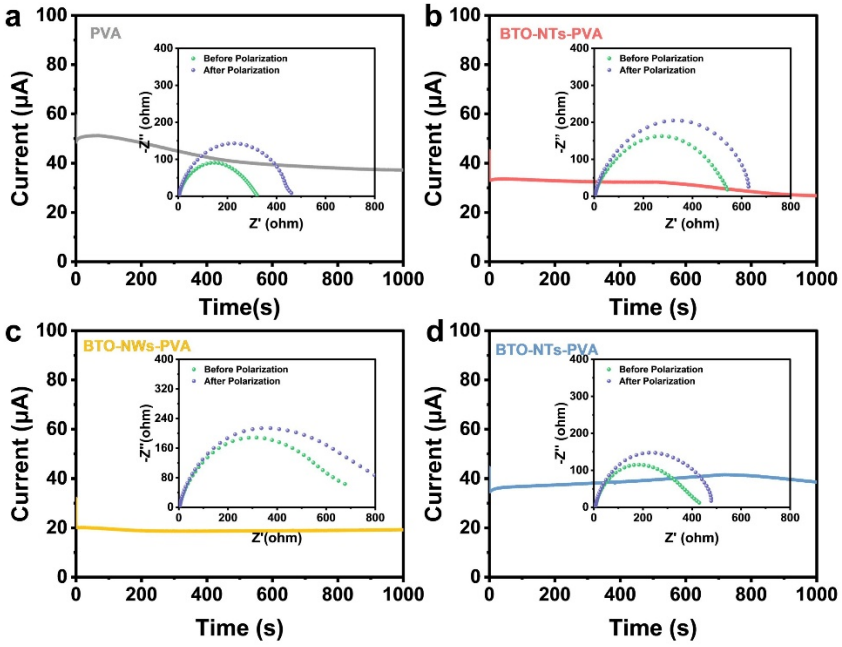

Figure S1. Zinc-ion transference number measurements for (a) PVA, (b) BTO-NTs-PVA, (c) BTO-NWs-PVA, and (d) BTO-NPs-PVA.

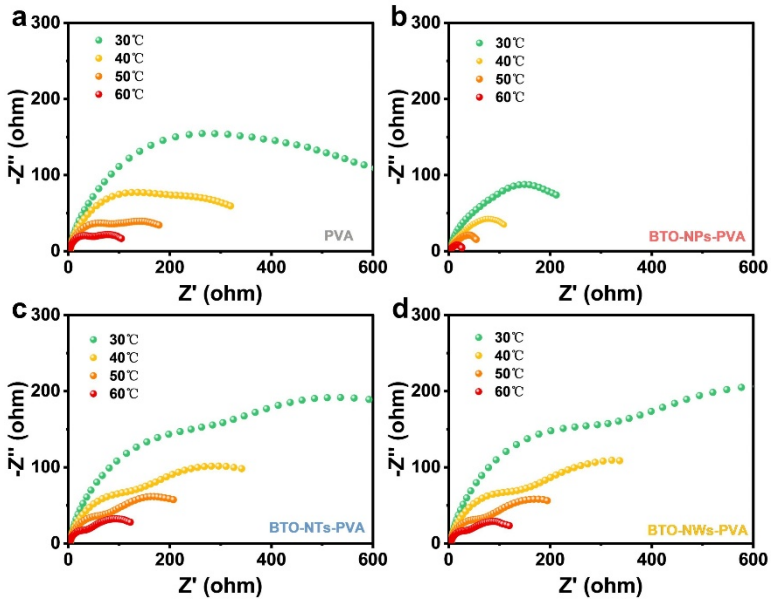

Figure S2. Activation energy measurements for (a) PVA, (b) BTO-NPs-PVA, (c) BTO-NTs-PVA, and (d) BTO-NWs-PVA.

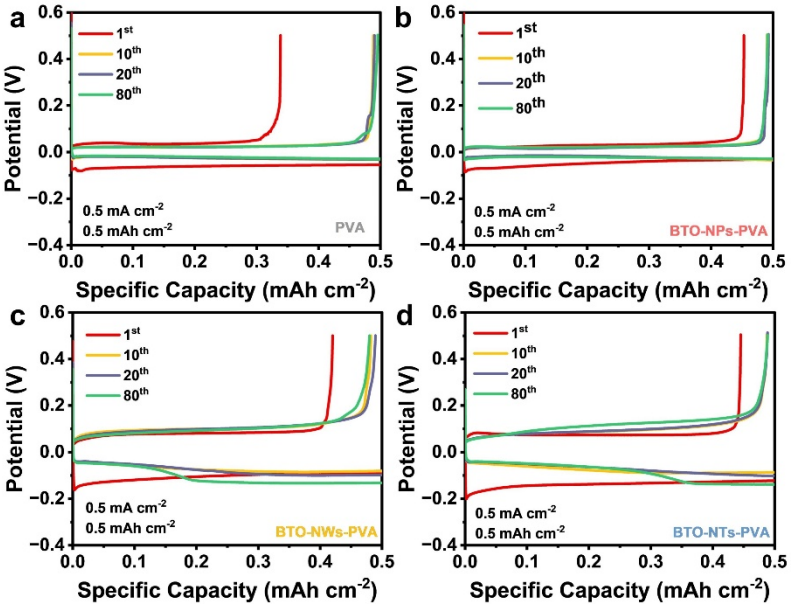

Figure S3. Specific capacity-voltage profiles for the first cycle of Zn||Cu half-cells with (a) PVA, (b) BTO-NPs-PVA, (c) BTO-NWs-PVA, and (d) BTO-NTs-PVA.

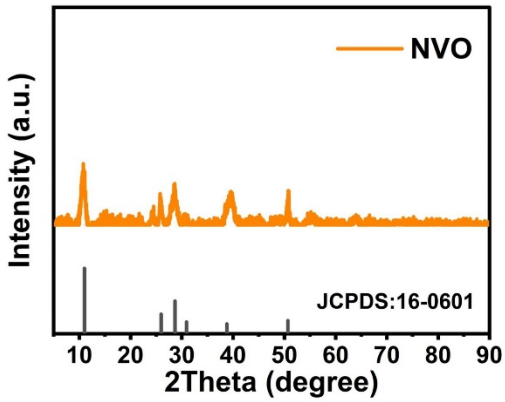

Figure S4. XRD pattern of the $NaV_3O_8 \cdot 1.5H_2O$ cathode material.

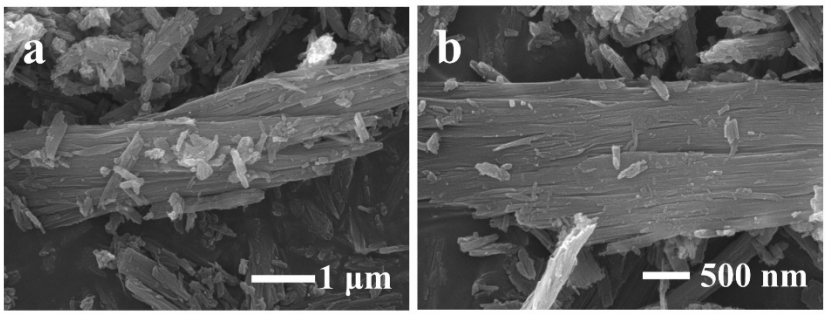

Figure S5. SEM image of the $NaV_3O_8 \cdot 1.5H_2O$ cathode material.

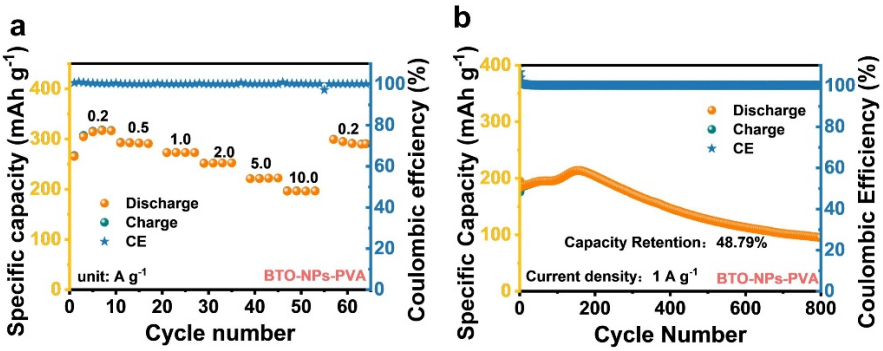

Figure S6. (a) Rate capability test and (b) long-term cycling test at 1.0 A g^{-1}.

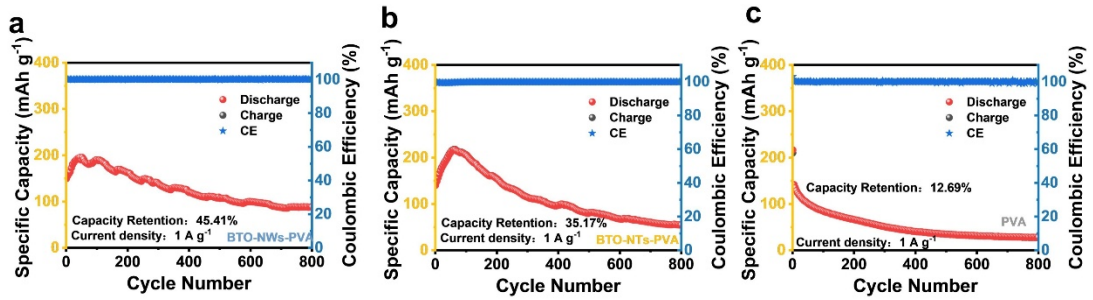

Figure S7. Long-term cycling test at 1.0 A g^{-1} for (a) BTO-NWs-PVA, (b) BTO-NTs-PVA, (c) PVA.